APPENDIX A

Nickel microparticles (99.8%; Goodfellow, London, UK) of a mean diameter 5.5 ± 1.8 μm with a hedgehog-like structure were coated with polypyrrole using an oxidative polymerization of pyrrole in aqueous solution.[29] The Ni particles were dispersed in a water solution containing pyrrole and methyl orange and after 10 minutes of stirring, ammonium peroxydisulfate solution was added under continuous stirring at room temperature. The final reaction mixture (200 mL) contained 0.1 M pyrrole, 0.125 M ammonium peroxydisulfate, 0.004 M methyl orange and 6 or 8 g of Ni. After 30 min the Nickel-polypyrrole particles were separated by filtration, sequentially rinsed with water and ethanol to remove any soluble species. The final product was a black powder which was left to dry at ambient temperature in open air for 48 h. Some of the key properties of the resulted particles are summarized below.

Fig. A1 depicts the morphology of the mixture of Nickel and polypyrrole. It is a relatively complicated structure, containing agglomerates of Ni particles completely coated with polypyrrole coating, which are connected by polypyrrole nanotubes with a diameter of 100–500 nm and a length of 5–10 μm on which globular polypyrrole particles are present. However, these agglomerates have a low cohesiveness and are broken by mixing.

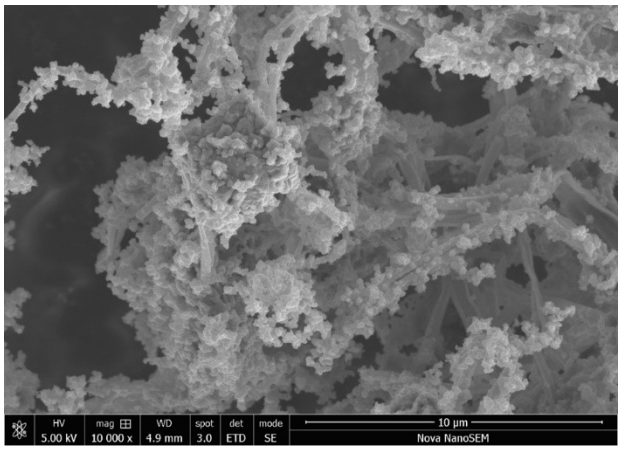

Fig. A1 SEM of nickel-polypyrrole mixture.

The electrical and magnetic properties of the Ni, Ni3, Ni4 and PPy particles are presented in Tab. A1 and are based on our previous work[29]. MRFs with 0.5 weight fraction were prepared based on the newly synthesized batch and were characterized in this work. The electrical properties were determined via the four-point van der Pauw method under 10kPa pressure using a lab made device and the magnetic properties from the magnetic hysteresis curve were extracted using vibrating sample magnetometry using the device Model 7407 from Lakeshore (USA). The saturation magnetization values of the MRFs are expected based on the weight fraction and the values of the pure particles further confirming the successful synthesis of the particles. The relatively high remanence justifies the creation of the aggregates but suggests weak attractive forces. The density of the Ni3 and Ni4 is expected to be 4.47 g/cm^3 and 5.06 g/cm^3 respectively, based on the weight fractions of Ni/PPy. For the calculation, the density of Ni was taken as 8.9 g/cm^3 provided from the supplied while for PPy the generally accepted value of 1.6 g/cm^3 was used.

Table. A1 The electrical and magnetic properties of MRFs and the components used during preparation.

	ρ (Ω cm)	σ (S/cm)	M_s (emu/g)	M_r (emu/g)
Ni3	5.1	0.196	39.3	2.00
Ni4	9.2	0.108	44.3	3.82
Ni	$1.43\ 10^{-3}$	699	53.3	0.2
PPy tubes	0.34	2.94	0.1	$2.6\ 10^{-6}$
MRFNi 3 Φ=0.5	-	-	19.1	0.782
MRFNi 4 Φ=0.5	-	-	22.5	0.915
MRFNi Φ=0.5	-	-	24.0	0.942

APPENDIX B

Electrorheological measurements were used to prove the presence of chain-like structures when an electric field is applied. The chain-like structures were only speculated given the particularly low electric fields used, ~2–3 orders of magnitude lower than in typical ERFs.[19] Under the corresponding magnetic fields, the chain-like structures were proven in a previous work.[29] To prove the internal chain formation mechanism within the investigated system also under an external electric field, the Anton Paar (model MRC 502, Austria) rotational rheometer in combination with the P-PTD200/E electro-cell were used. A parallel plate geometry with a 25mm diameter was employed. Electric fields were generated through the HCP 14-12500MOD, high voltage supply unit. For the investigation of the ER behaviour, the samples were subjected to a steady shear at the very low shear rate of 0.1 1/s to better simulate the behaviour inside the measuring cell where the MRFs were at rest (section 3). During shearing, the electric field was turned on and off every 20 seconds with the field values being increased in a step-wise manner. Due to the low voltages used, their values were slightly fluctuating resulting in a ~10% error for values of the electric field which were calculated by averaging the corresponding fields. All measurements were performed at room temperature. Before each measurement, the samples were sheared at 20 1/s for a

minute to redisperse the particles and break potential agglomerates.

The effect of step-wise increase of the electric field on the MRF4 is shown in Fig. B1 (a). As can be seen, when an electric field is applied, the shear stress values are notably increased due to the arrangement of the particles into chain-like structures. At higher fields, the stress is further increased as the chain-like structures become more robust. When the field is turned off, the stress is gradually reduced, however not reaching the initial off-state values further supporting the potential of a residual polarization referred in section 3.

Both suspensions were compared in terms of their ER effects given by the following formula:

$$ER\ effct = \frac{\tau_{on} - \tau_{off}}{\tau_{off}} \cdot 100\% \quad \text{(E1)}$$

where τ_{on} and τ_{off} being the shear stress during the on- and off-state. To calculate the abovementioned quantities, the average values for τ_{on} were used for a given field, while for the τ_{off}, the data of the first 20 seconds were averaged. In Fig. E1 (b) the ER effects for both MRFs are shown. The trend is similar to conductivity in Fig. 7 with MRF4 showing a significantly higher ER effect due to the enhanced dipole-dipole interactions. For the MRF3 the ER effect is relevantly low, nevertheless its existence proves the presence of chain-like structures within that suspension. The MRF4 on the other hand, obtained impressive values of ER effect compared to other systems.[19] In spite of that, these systems perform under very low electric fields in the range of a kV/m while typical ER fluids operate in the range of a few kV/mm. Thus, our systems need significantly lower voltages to operate, consequently, being more efficient and economical.

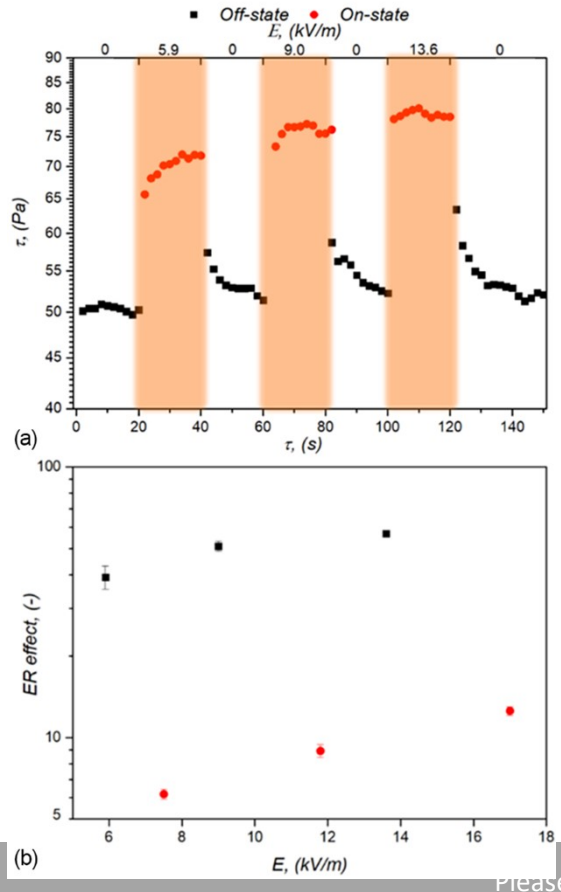

Fig. B1. (a) Effect of step-wise increase of the *E* field during steady shear at 0.1 Hz for MRF4. (b) ER effect for MRF3 (red spheres) and MRF4 (black squares).

APPENDIX C

Summary of the coefficients obtained from the quadratic fits from Eq. (1) of current intensity data for both MRF3 and MRF4 samples in Fig. 6(a) and (b). In the initial unconstrained fit of Eq. (1) for the case *B*=0, the parameter I_{0em} was found to be slightly positive (0.498 μA), which is inconsistent with the experimentally observed negative baseline current at zero field (see Fig. D1). To ensure physical consistency with the measured behaviour of the suspension in the absence of an applied electric field, we re-fitted the data under the constraint $I_{0em} \leq 0$. The revised fit yielded I_{0em}=0.000 μA with updated values for the remaining parameters: α=0.506 nSm and β=0.191 pS^{2}m^2/A. This constrained model better reflects the residual polarization state of the suspension and removes the unphysical sign reversal of I_{0em} noted in earlier fits. The revised values are included in Tab. C1.

Table C1 Coefficients I_{0em}, α and β, and coefficient of determination *R*-squared obtained by fitting data in Fig. 6(a) with Eq. (1).

B	I_{0em} (μA)	α (nSm)	β (pS^2m^2/A)	*R*-squared (-)
0	0.000	0.506	0.191	0.99993
30	-11.806	57.504	1.327	0.99997
60	-18.808	80.685	1.381	0.99998
90	-23.065	102.337	1.455	0.99999

Table C2 Coefficients I_{0em}, α and β, and coefficient of determination R-squared obtained by fitting data in Fig. 6(b) with Eq. (1).

B	I_{0em} (μA)	α (nSm)	β (p$S^2m^2A^{-1}$)	*R*-squared (-)
0	-4.891	31.206	1.234	0.99997
30	-11.806	57.504	1.327	0.99997
60	-18.808	80.685	1.381	0.99998
90	-23.065	102.337	1.455	0.99999

APPENDIX D

During the current intensity measurements for both MRFs, in the absence of electric field and up to approximately 0.5 kV/m, the measured current values were observed to be negative (Fig. D1). As the electric field was being increased beyond this threshold, the current intensity became positive. This behaviour can be attributed to the initial electrical polarization of the microparticles within the composite, which generated a spontaneous internal voltage. This internal voltage, likely resulting from residual polarization effects or partial dipole alignment, acted against the externally applied electric field, causing a negative current through the internal resistance of the composite. As the external electric field strength was being increased and surpassed the spontaneous voltage, the current direction was reversed to positive. This phenomenon is quantitatively reflected in the model by I_{0em} (Tab. C1 and C2), which represents the baseline current in the absence of an external field. The higher value of I_{0em} observed in MRF4 compared to MRF3 suggests a more significant residual polarization, consistent with the higher Ni content and stronger initial dipole interactions in MRF4. Note that the deviation of the I_{em} values at $E = 0\ kV/m$ of Fig. D1 deviate from the I_{0em} values in Tab. B1 and B2 are expected as at such low *E* fields, the alignment of the particles was unlikely, something that the current model from, Eq. (1) does not take into account.

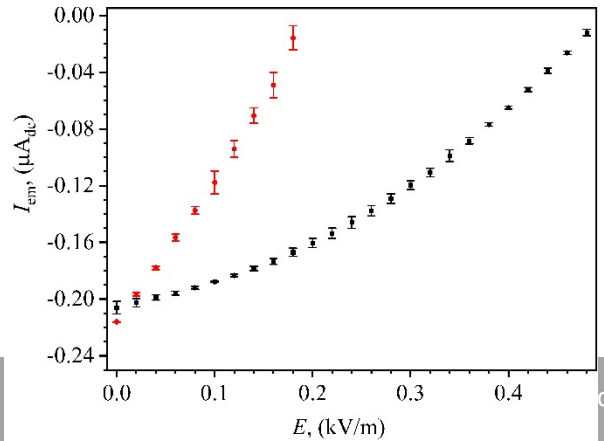

Fig. D1. The average intensity of the electric current through the suspensions MRF3 (black) and MRF4 (red) at very small values of electric field.

APPENDIX E

Summary of the coefficients obtained from the quadratic fits from Eq. (4) of current intensity data for both MRFs in Fig. 7 (a) and (b). The high R-squared values indicate very good fits.

Table E1 Coefficients σ_{0em}, γ and δ, and coefficient of determination *R*-squared obtained by fitting data in Fig. 7 (a) with Eq. (4).

B	σ_{0em} (10^{-6} $\Omega^{-1}m^{-1}$)	γ (10^{-6} $\Omega^{-1}kV^{-1}$)	δ (10^{-6} $kV\Omega^{-1}m^{-2}$)	***R*-squared (-)**
0	1.776	0.592	0.184	0.99984
30	9.356	1.282	-2.270	0.99997
60	25.154	2.083	-5.959	0.99996
90	38.101	2.509	-8.531	0.99997

Table E2 Coefficients σ_{0em}, γ and δ, and coefficient of determination *R*-squared obtained by fitting data in Fig. 7(b) with Eq. (4).

B	σ_{0em} ($\Omega^{-1}m^{-1}$)	γ ($\Omega^{-1}kV^{-1}$)	δ (10^{-6} $kV\Omega^{-1}m^{-2}$)	***R*-squared (-)**
0	99.533	3.917	-15.682	0.99997
30	178.693	4.535	-27.354	0.99998
60	248.819	4.963	-41.140	0.99996
90	316.277	5.303	-51.419	0.99995